THE JOURNAL OF BIOLOGICAL CHEMISTRY
Vol. 278, No. 23, Issue of June 6, pp. 20925–20933, 2003

*Printed in U.S.A.*

# Functional Insensitivity of the Cytochrome $b_6f$ Complex to Structure Changes in the Hinge Region of the Rieske Iron-Sulfur Protein*

Received for publication, December 11, 2002, and in revised form, March 13, 2003
Published, JBC Papers in Press, April 2, 2003, DOI 10.1074/jbc.M212616200

**Jiusheng Yan and William A. Cramer‡**

*From the Department of Biological Sciences, Purdue University, West Lafayette, Indiana 47907-2054*

**Structure analysis of the cytochrome $bc_1$ complex in the presence and absence of $Q_p$ quinol analog inhibitors implied that a large amplitude motion of the Rieske iron-sulfur protein (ISP) is required to mediate electron transfer from ubiquinol to cytochrome $c_1$. Studies of the functional consequences of mutagenesis of an 8-residue ISP "hinge" region in the $bc_1$ complex showed it to be sensitive to structure perturbation, implying that optimum flexibility and length are required for the large amplitude motion. Mutagenesis-function analysis carried out on the ISP hinge region of the cytochrome $b_6f$ complex using the cyanobacterium *Synechococcus* sp. PCC 7002 showed the following. (i) Of three *petC* genes, only that in the *petCA* operon codes for functional ISP. (ii) The function of the complex was insensitive to changes in the hinge region that increased flexibility, decreased flexibility by substitutions of 4–6 Pro residues, shortened the hinge by a 1-residue deletion, or elongated it by insertion of 4 residues. The latter change increased sensitivity to $Q_p$ inhibitors, whereas deletion of 2 residues resulted in a loss of inhibitor sensitivity and a decrease in activity, indicating a minimum hinge length of 7 residues required for optimum binding of ISP at the $Q_p$ site. Thus, in contrast to the $bc_1$ complex, the function of the $b_6f$ complex was insensitive to sequence changes in the ISP hinge that altered its length or flexibility. This implies that either the barriers to motion or the amplitude of ISP motion required for function is smaller than in the $bc_1$ complex.**

The cytochrome $b_6f$ complex functions as a plastoquinol: plastocyanin/cytochrome $c_6$ oxidoreductase in oxygenic photosynthesis and is shared by both photosynthetic and respiratory electron transfer pathways in cyanobacteria (1). It mediates electron transfer from photosystem II to photosystem I in the linear electron transfer pathway or around photosystem I in a cyclic pathway, generating an electrochemical proton gradient across the membrane that is used for the synthesis of ATP (2, 3). The $b_6f$ complex is phylogenetically analogous to the cytochrome $bc_1$ complex of mitochondria and photosynthetic bacteria. It is an integral membrane protein complex composed of eight to nine polypeptide subunits (3, 4), the four largest (>17 kDa) of which have defined functions. The 24-kDa cytochrome $b_6$ subunit, which has four transmembrane $\alpha$-helices and contains two b-type hemes, together with the 17-kDa subunit IV, which has three transmembrane helices, are homologous to the N- and C-terminal segments of the cytochrome $b$ in the $bc_1$ complex (5). The 19-kDa Rieske iron-sulfur protein (ISP),[1] consisting of an N-terminal single transmembrane $\alpha$-helix domain and a 140-residue soluble extrinsic domain with a linker region connecting these two domains, has an overall function similar to that of the ISP in the $bc_1$ complex, deprotonating the membrane-bound quinol and transferring electrons from the quinol to the membrane-bound $c$-type cytochrome (6–8). Of the two subdomains of the ISP extrinsic domain, the cluster-binding small subdomain involved in formation of the $Q_p$ site (the quinone-binding site on the electrochemically positive side of the $b_6f/bc_1$ complex) is structurally identical in the two complexes, whereas the large subdomain, which is directly connected to the linker region, has a different fold (9). In addition, the structure of the membrane-bound $c$-type cytochrome is completely different in the two complexes. The 31-kDa $c$-type cytochrome $f$ subunit is functionally related to, but structurally completely different from, the cytochrome $c_1$ in the $bc_1$ complex (10, 11). The structure differences, as well as the similarities, between these two complexes are important for understanding the mechanism of the ISP in the $b_6f$ complex (see below).

High resolution x-ray diffraction analysis of the mitochondrial cytochrome $bc_1$ complexes in the presence/absence of the $Q_p$ site inhibitor stigmatellin suggested an intracomplex electron shuttle function for the ISP subunit, which mediates electron transfer from ubiquinol at the $Q_p$ site to cytochrome $c_1$ through a 60° rotation of its extrinsic soluble domain and a resulting 16-Å displacement of the [2Fe-2S] cluster (Fig. 1) (7, 12–16). In the crystal structures, the displacement of the ISP extrinsic domain is accompanied by a large conformational change in the hinge region (flexible part of the linker region), whereas the internal structure of the extrinsic domain and the position of the membrane anchor domain are little changed at ~3-Å resolution (Fig. 1) (12, 14). It was subsequently found that the function of the complex is very sensitive to perturbation of the sequence and structure of the hinge region by site-directed mutagenesis in which the hinge was altered by residue deletion, insertion, and substitution (17–26). Although these data were interpreted in terms of a requirement for the mobility of the ISP soluble domain, the extreme sensitivity of $bc_1$ function to increases in hinge flexibility (19) and length (17, 24, 26) cannot be predicted or inferred from the x-ray structure data. Thus, it is of interest to study the function of the putative hinge region in the $b_6f$ complex (Table I).

Because the structure of the ISP and the predicted structures of the cytochrome $b_6$ and subunit IV in the $b_6f$ complex

* This work was supported by National Institutes of Health Grant GM-38323. The costs of publication of this article were defrayed in part by the payment of page charges. This article must therefore be hereby marked "*advertisement*" in accordance with 18 U.S.C. Section 1734 solely to indicate this fact.

‡ To whom correspondence should be addressed. Tel.: 765-494-4956; Fax: 765-496-1189; E-mail: wac@bilbo.bio.purdue.edu.

[1] The abbreviations used are: ISP, iron-sulfur protein; DBMIB, 2,5-dibromo-3-methyl-6-isopropyl-*p*-benzoquinone.

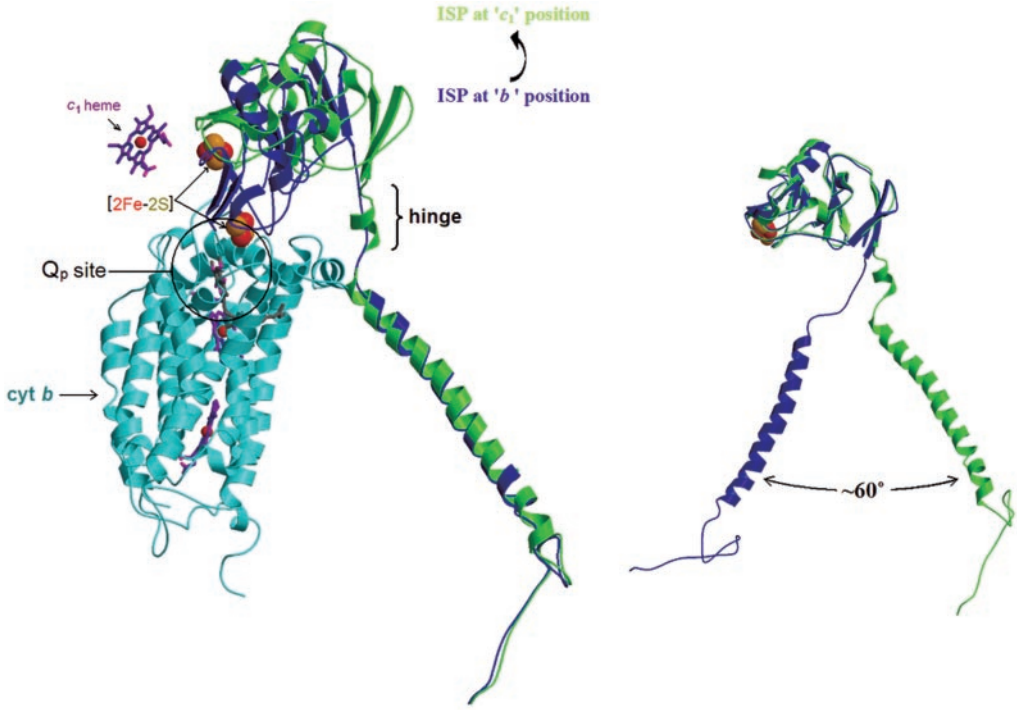


FIG. 1. **The two extreme positions of the ISP extrinsic domain and the corresponding conformational changes in the hinge region of the avian cytochrome $bc_1$ complex (12).** The ISP located at the $b$ position is shown in *blue*, and that at the $c_1$ position in *green*. *Left*, two different positions of ISP in the context of the cytochrome (*cyt*) $b$ subunit and cytochrome $c_1$ heme; *right*, artificial superposition of the ISP extrinsic domain at its two extreme positions, to demonstrate that its motion involves a ~60° rotation. Structures were drawn with MOLSCRIPT (49) and RASTER3D (50).

are similar to the structures of the ISP and cytochrome $b$ in the $bc_1$ complex, it is expected that the ISP in the stigmatellin- or DBMIB-bound $b_6f$ complex is in a position and orientation similar to those observed in the stigmatellin-bound $bc_1$ complex (Fig. 2). Three lines of evidence indicate that the ISP in the $b_6f$ complex may also act as a mobile redox center. (i) EPR studies defined different orientations for the [2Fe-2S] cluster of the ISP extrinsic domain in the presence and absence of the $Q_p$ site quinol analog inhibitor DBMIB (27) or inhibitory metal ions (28). (ii) The rate of flash-induced reduction of cytochromes $b_6$ and $f$ is systematically inhibited as a function of ambient extrinsic viscosity *in situ* (29). (iii) An 8-residue segment containing 4–7 Gly, 0–3 Ser, 0–1 Thr, and 0–2 Ala residues, whose alignment with the set of Rieske ISP sequences suggests that it is a putative hinge region, is present in the $b_6f$ complex (Table I). The sequence of this segment is conserved in the ISP sequences of $b_6f$ complexes from various organisms (Table I) and suggests a higher degree of conformational flexibility than in the $bc_1$ complex. Thus, it is anticipated that a movement of the ISP soluble domain is involved in electron transfer from quinol to cytochrome $f$ in the $b_6f$ complex. To probe the role of the putative ISP hinge region in the $b_6f$ complex, the cyanobacterium *Synechococcus* sp. PCC 7002, previously used for site-directed mutagenesis of cytochrome $b_6$ and subunit IV (30), was used for mutagenesis of the ISP. In contrast to the $bc_1$ complex, the function of the $b_6f$ complex was found to be insensitive to large perturbations of the ISP hinge region, implying major differences between the complexes either in structural barriers to motion of the ISP soluble domain or in the amplitude of its motion.

## MATERIALS AND METHODS

*Growth of Cultures*—*Synechococcus* sp. PCC 7002 wild-type and mutant strains were grown in medium A (31) supplemented with spectinomycin at 100 $\mu$g/ml for mutants. Liquid cultures were grown at 38 °C under cool-white fluorescent illumination at a light intensity of ~100 microeinsteins/m$^2$/s, bubbled with air supplemented with ~2.0% (v/v) $CO_2$. Cell densities were determined from the absorbance at 730 nm.

*Site-directed Mutagenesis and Plasmid Construction*—A PCR-based site-directed mutagenesis method (Stratagene) was performed as described (32). The presence of mutations and the intactness of the remainder of the *petC1* genes on plasmids and in the *Synechococcus* genome were analyzed by DNA sequencing. For mutants 4Pro, 6Pro, and +4G, the intactness of their genomic *petB* and *petD* genes, which encode cytochrome $b_6$ and subunit IV, was confirmed by sequencing. A 3.5-kb segment encompassing the *petCA* operon and 1.5 kb of the 5′-flanking sequence was digested from pUHWRW1 (33) with *Xba*I and *Kpn*I and cloned into the *Xba*I and *Kpn*I sites of pUC19 to generate plasmid I. A *Hin*dIII site (silent mutation) was introduced into the 3′-end of the *petC1* gene by site-directed mutagenesis with CTG TCC AGT CGG TGA AGC TTC ACC GAC TGG ACA G (mutation sites are underlined) and its complementary primer to generate plasmid II, which was digested with *Hin*dIII; and the resulting 4.5-kb segment was cyclized by ligation to generate plasmid III. A new *Pac*I site was introduced at a site ~30 bp upstream of the *petC1* start codon by mutagenesis with GGA AGT ATT GTA GAA ACG CTT AAT TAA CTA TAC AAA AGG CTC TG and its complementary primer. The resulting plasmid IV was linearized at a site ~500 bp upstream of *petC1* by PCR with *Pfu* polymerase and primers GGC CCG TTC TCC CAA TTC C and GGC AGA ATG GCT GTT GGG TTA ATC C. The *aadA* cassette (34), which encodes an aminoglycoside 3′-adenyltransferase and confers spectinomycin resistance to the host strains, was ligated with the linearized plasmid IV to generate plasmid V, which contains an *aadA* cassette located ~500 bp upstream of *petC1*. A 3.8-kb fragment including the 5′-part of *petC1* and the 5′-flanking sequence with the *aadA* cassette was excised from plasmid V by restriction digestion with *Pml*I and *Bam*HI and ligated into the *Pml*I and *Bam*HI sites of plasmid I to generate plasmid pCA1, which contains the whole *petCA* operon and an inserted *aadA* cassette (2.0 kb) in its 5′-flanking sequence (1.5 kb). This was the final plasmid used to transform the *Synechococcus* cells. pCA1 was digested with *Pml*I and *Hpa*I to remove the 5′-flanking sequence and then religated to create construct pCA2. Mutations in *petC1* were first made on plasmid pCA2 by site-directed mutagenesis, and then the *petCA* operon containing the desired mutation was excised from pCA2 by *Pac*I and *Xba*I digestion and cloned into the *Pac*I and *Xba*I sites of pCA1 to generate the pCA1 mutant.

To delete the *petC1* gene in the *petCA* operon, *Pml*I and *Sma*I unique sites were introduced at the 5′- and 3′-ends of *petC1* by site-directed mutagenesis with CT ATA CAA AAG GCT CTG ATT ATG CAC GTG

TABLE I

*Sequence alignment of the ISP hinge region in the cytochrome $bc_1$ and $b_6f$ complexes*

Asterisks indicate invariant residues; colons indicate highly conserved residues; and periods indicate conserved residues.

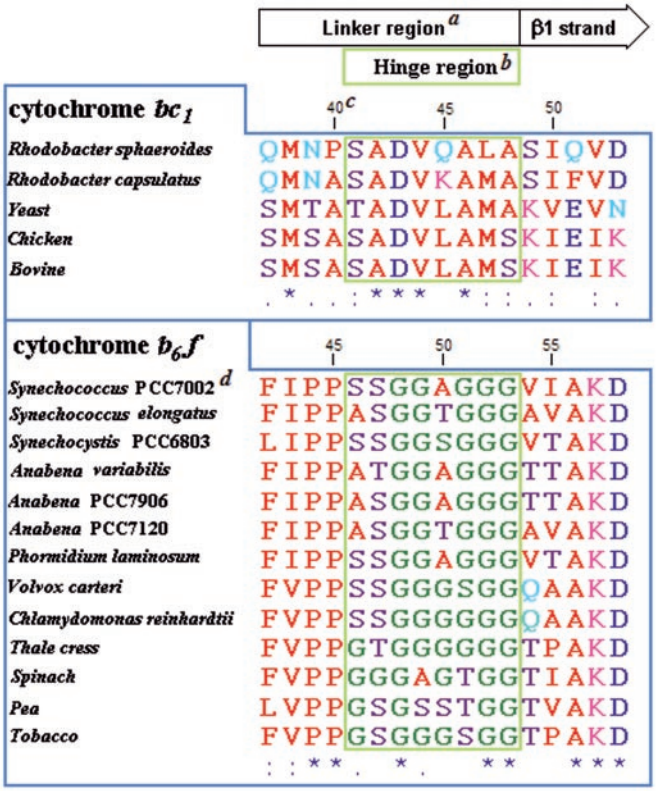


[a] Start and stop residues of the ISP linker region and its hinge region in the $bc_1$ complex are based on the ISP structures in the complex (12, 14, 15) and the truncated soluble form (51). The spinach Phe[41] site (Phe[42] in *Synechococcus* PCC 7002), where soluble ISP was proteolyzed from the complex by thermolysin (52), is used as the start site of the linker region in the $b_6f$ complex. Prediction of the stop site is based on the structure of the soluble domain of spinach ISP using the start of the first β-strand (9).

[b] The hinge region is the conformationally flexible segment.

[c] Residue number is for the first organism in the alignment.

[d] For cyanobacterial sequences, only the amino acid sequence deduced from the *petC* gene in the *petCA* operon is reported.

ACT CAA TTA TCA GGT TCC T and C CGT ACT GAC GAA GCT CCC GGG TGG GCC TAA AAA CCC CAT ACG and their complementary primers. The resulting pCA2 mutant was digested with *Pml*I and *Sma*I to remove *petC1* and religated to generate plasmid pCA2-Δ*petC1*. The *petCA*-Δ*petC1* operon was then excised from pCA2-Δ*petC1* and cloned into pCA1 to generate pCA1-Δ*petC1*. Mutations in the ISP hinge region were made by site-directed mutagenesis with the following primers (complementary primers not shown): P44A/P45A, CCC GTT ATT AAA TAT TTT ATT GCT GCT TCT AGT GGT GGC; S46G/S47G, GTT ATT AAA TAT TTT ATT CCT CCT GGT GGT GGT GGC GCT GGT GG; 4Pro, CCT CCT TCT AGT GGT CCC CCT CCT CCT GGC GTG ATT GC; 6Pro, CCC GTT ATT AAA TAT TTTT ATT CCT CCT CCT CCT GGT CCC CCT CCT CCT GGC; ΔA50, CCT CCT TCT AGT GGT GGC_GGT GGT GGC GTG ATT GC; ΔS46–47, GTT ATT AAA TAT TTT ATT CCT CCT__GGT GGC GCT GGT GGT GG; ΔG51–52, CCT CCT TCT AGT GGT GGC GCT__GGC GTG ATT GCT AAA GAT GCC; +2G-Δ2G, CCC GTT ATT AAA TAT TTT ATT CCT CCT GGC GGC TCT AGT GGT GGC GCT__GGC GTG; and +4Gly, CCT TCT AGT GGT GGC GCT GGT GGC GGC GGT GGT GGC GGC GTG ATT GC.

*Transformation of Synechococcus Cells and Screening of Complete Segregants*—Transformation of *Synechococcus* PCC 7002 with plasmid was performed as described (30, 31), except that, after incubation of the plasmid with cells at 37 °C under light for 90 min, the plasmid/cell mixture was applied to medium A plates supplemented with 100 μg/ml spectinomycin. After 7–10 days of incubation, spectinomycin-resistant transformants appeared and were streaked on spectinomycin plates for further segregation. The primary screening for the complete segregants with the desired mutation in the *petC1* gene of the *Synechococcus* genome was performed by PCR and subsequent restriction analysis of the PCR product (see Fig. 3*A*). *Synechococcus* genomic DNA for PCR was extracted as described (30, 35). A 1-kb fragment containing *petC1* and the 5′-part of *petA* was amplified with a forward primer (GGG CAA ACT AAG GCT C) and a reverse primer (AAA CTT GAT CGG GTA AAA CGG). The PCR product was digested with *Hin*dIII and then analyzed by agarose gel electrophoresis. Complete digestion of the PCR product with *Hin*dIII indicated complete segregation and absence of the wild-type allele in the *Synechococcus* genome. The presence of the desired mutations in the *petC1* gene of the *Synechococcus* genome and complete segregation were confirmed by sequencing of the PCR products that could be completely digested with *Hin*dIII.

*Oxygen Evolution*—Oxygen evolution rates were measured at 39 °C with a Clark-type oxygen electrode and a saturating actinic light intensity of 2000–2500 microeinsteins/$m^2$/s. Cells harvested in late log phase were suspended at a chlorophyll concentration of 10 μg/ml in 5 mM HEPES (pH 7.5), 10 mM NaCl, and 10 mM $NaHCO_3$.

*Flash Kinetic Spectroscopy*—The electron transfer activity of the cytochrome $b_6f$ complex *in vivo* was measured in terms of the rate of flash-induced re-reduction of cytochromes *f* and $c_6$ in their α-band absorption region ($\Delta A_{556-540\ nm}$) using a spectrometer as described (36). *Synechococcus* cells were harvested in late log phase and kept in darkness. Prior to measurement, cells were suspended at 5 μM chlorophyll in reaction medium consisting of 5 mM HEPES (pH 7.5), 10 mM NaCl, and 10 mM $NaHCO_3$. 10 μM 3-(3,4-dichlorophenyl)-1,1-dimethylurea, 1 mM $NH_2OH$, and 10 μM carbonyl cyanide *p*-trifluoromethoxy-phenylhydrazone were added to dissipate flash-induced absorbance changes from photosystem II and to disrupt the transmembrane electrochemical potential. To eliminate variation in the redox state of the plastoquinone pool in the dark, 1.0 mM KCN was incubated at room temperature (1 min) to block respiration.

*Homology Modeling of the Cytochrome $b_6f$ Complex*—From the sequence similarity between the cytochrome *b* in the $bc_1$ complex and cytochrome $b_6$/subunit IV and the positions of the invariant residues (5, 37), it has been concluded that cytochrome $b_6$ and subunit IV should have the same general structure as the N- and C-terminal domains of the mitochondrial cytochrome *b* (5, 37). Also, from the high degree of sequence conservation observed around the $Q_p$ site that contacts the ISP and the nearly identical primary and tertiary structures of the cluster-binding ISP small subdomain in chloroplasts and mitochondria (9, 37), the ISP in the stigmatellin-bound $b_6f$ complex should be in a similar position and orientation as observed in the stigmatellin-bound $bc_1$ complex. Therefore, three of the four large subunits in the $b_6f$ complex can be modeled within the complex, whereas the position of the unique cytochrome *f* is not known. A model of the $b_6f$ complex in which the ISP is located at the $Q_p$ site and cytochrome *f* is excluded was built by homology modeling with SWISS MODEL and SWISS-pdb viewer (38). The crystal structure of the yeast $bc_1$ complex with stigmatellin (Protein Data Bank code 1EZV) (15) was used as a template for the homology modeling. The structure of the *Synechococcus* ISP soluble domain was modeled from the crystal structure of the spinach ISP soluble domain (Protein Data Bank code 1RFS) (9) and superimposed on the complex based on the structural similarity of the cluster-binding small subdomains between the mitochondrial and chloroplast ISPs (9).

## RESULTS

*The petC1 Gene Encodes Functional ISP*—The ISP of the $b_6f$ complex is encoded by the *petC* gene in higher plants and cyanobacteria. Originally, only one *petC* gene (*petC1*), which is located in the *petCA* operon, was reported for *Synechococcus* sp. PCC 7002 (33). However, a BLAST search in the recently deposited genome (NCBI accession number NC_003488) indicated that, as in *Synechocystis* sp. PCC 6803 (39), there are two additional *petC* genes (*petC2* and *petC3*) in the *Synechococcus* genome. In *Synechocystis*, the *petC* gene located in the *petCA* operon was shown to be the dominant species in membranes and in isolated $b_6f$ complex by immunoblotting (39). To study the function of PetC1 and its hinge region, a Δ*petC1* mutant with the entire *petC1* gene deleted and nine hinge region mutants with changes in the composition, flexibility, and length of the hinge region were constructed (Table II).

The cytochrome $b_6f$ complex is required for both respiration and photosynthesis in cyanobacteria; therefore, only non-lethal

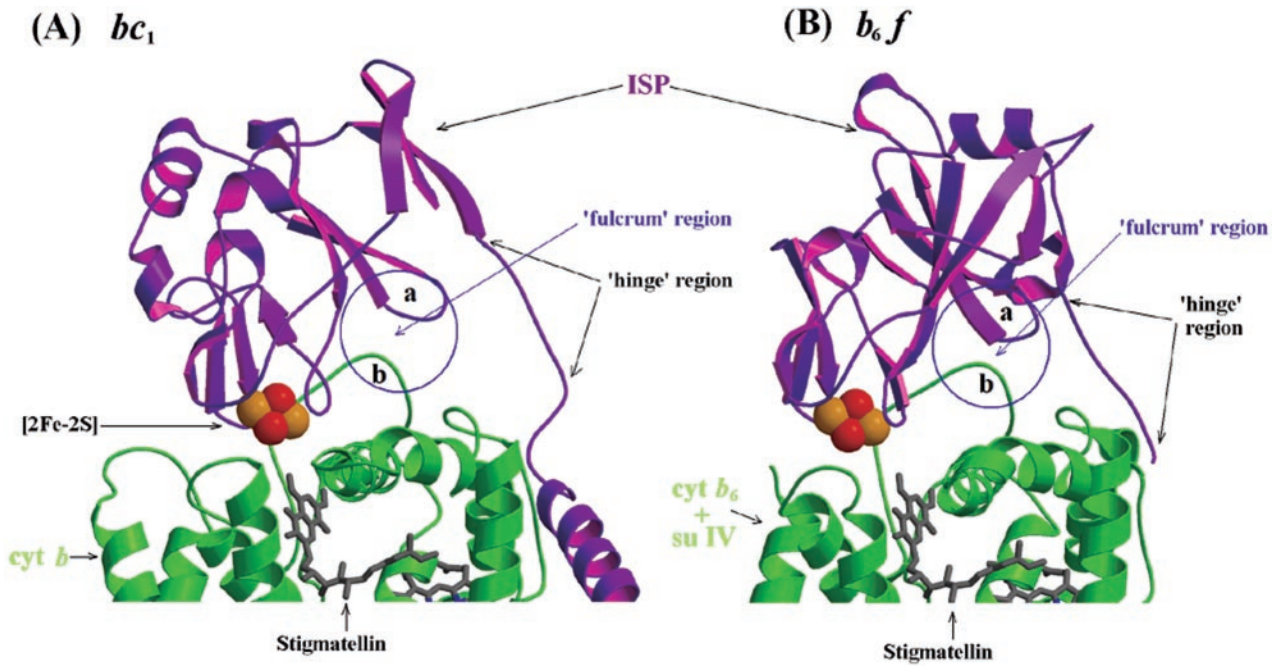


FIG. 2. **Interaction of the ISP soluble domain with the *p* side of cytochrome *b* in the stigmatellin-bound avian $bc_1$ complex (12) (*A*) and of cytochrome $b_6$ and subunit IV in the modeled structure of the $b_6f$ complex (*B*).** The contact between the $\beta_{2-3}$-strand region (site *a*) of the ISP and the *ef* loop (site *b*) of cytochrome (*cyt*) *b* in the $bc_1$ complex or between cytochrome $b_6$ and subunit (*su*) IV in the $b_6f$ complex is labeled as a fulcrum region and highlighted by a *blue circle*. Structures were drawn with MOLSCRIPT (49) and RASTER3D (50).

mutants can be propagated and segregated from the wild-type allele, and deleterious mutations are detected as non-segregants. All hinge region mutants reported in this study (listed in Table II) were segregated completely from the wild type. The PCR products of their genomic *petC1* genes could all be digested completely with *Hin*dIII (Fig. 3*B*, *lanes 2–9*) (data for mutant 6Pro not shown). All these mutants grew well under photosynthetic conditions with a growth rate (doubling time of 4.5–6.2 h) similar to that of the wild type (doubling time of 5.4 h) (Table II). Analysis of the content of the $b_6f$ complex in membranes by Western blotting and heme staining indicated that the assembly and stability of the $b_6f$ complex were not significantly affected in these mutants (data not shown). On the contrary, no segregant could be obtained for the Δ*petC1* mutant. Thus, both wild-type and Δ*petC1* alleles were present in the PCR products of non-segregants (Fig. 3*B*, *lane 10*), implying an essential role of the *petC1* gene product for *Synechococcus* sp. PCC 7002. In addition, certain mutations (*e.g.* deletion of $Gly^{51}$ and $Gly^{52}$) in the PetC1 hinge region caused a significant decrease in the electron transfer activity of the $b_6f$ complex and a loss of its sensitivity to DBMIB (discussed below), suggesting a dominant role of PetC1 in the function of the $b_6f$ complex. Therefore, it was concluded that *petC1* codes for the essential ISP in *Synechococcus* sp. PCC 7002, whereas *petC2* and *petC3* are silent in the function of the $b_6f$ complex. This makes it practical to analyze the structure and function of the ISP by mutagenesis of *petC1* without knockout of *petC2* and *petC3* in *Synechococcus* sp. PCC 7002.

*Flash-induced Cytochrome $f/c_6$ Kinetics*—In *Synechococcus* sp. PCC 7002, cytochrome $c_6$, instead of plastocyanin, whose gene cannot be found in the genome (NCBI accession number NC_003488), mediates electron transfer from the cytochrome $b_6f$ complex to photosystem I. The electron transfer activity of the cytochrome $b_6f$ complex *in vivo* can be measured in terms of the rate of flash-induced re-reduction of cytochromes *f* and $c_6$ in their α-band absorption region by a flash spectrometer with intact *Synechococcus* cells (30, 40). A light-dark difference spectrum of flash-induced absorbance changes in the region at 540–570 nm clearly shows the absorbance changes to consist of contributions from both cytochromes *f* (α-band maximum, 556 nm) and $c_6$ (α-band maximum, 553 nm) (data not shown). The observations in this study that (i) deletion of 2 residues at two different positions in the hinge region produced similar effects on the kinetics of cytochromes *f* and $c_6$ and (ii) the retardation of the cytochrome $f/c_6$ reduction and the loss of its sensitivity to inhibitors in mutant ΔG51–52 could be fully reverted by reinsertion of 2 Gly residues at a second site between $Pro^{45}$ and $Ser^{46}$ in a "restoration mutant," +2G-Δ2G (Fig. 4 and Table II; discussed below), show that the flash-induced absorbance change in this region is fully attributed to the electron transfer activity of the $b_6f$ complex.

*Consequences of Increased Flexibility and Length of the Hinge Region*—It has been shown in *Rhodobacter capsulatus* that introduction of excess flexibility by substitution with 6 Gly residues (19) or of extra length by insertion of 1 or more residues (17, 24, 26) in the hinge region is deleterious to the function of the $bc_1$ complex (Table III, parts A and B). With 4–7 glycine residues in the sequence, the ISP hinge region in the $b_6f$ complex is predicted to be structure-less and more flexible than that in the $bc_1$ complex (Table I). Further increases in flexibility or length caused by changing $Pro^{44}$ and $Pro^{45}$, which are conserved at the N-terminal end of the hinge region but absent in the $bc_1$ sequences, to 2 Ala residues in mutant P44A/P45A or $Ser^{46}$ and $Ser^{47}$ to 2 Gly residues in mutant S46G/S47G or by insertion of 4 extra Gly residues in mutant +4Gly (resulting in a total of 9 Gly residues in the "hinge" region) had no effect on the activity of the complex. These mutants showed an electron transfer activity ($t_{½}$ of cytochrome $f/c_6$ reduction = 3.1–5.2 ms) similar to that of the wild type ($t_{½}$ of cytochrome $f/c_6$ reduction = 4 ms) (Fig. 4 and Table II). Therefore, it is concluded that, in contrast to the $bc_1$ complex, extreme flexibility and extra length of the hinge region are well accommodated in the $b_6f$ complex (Table III, parts A and B).

*Effect of Decreased Flexibility*—In the bacterial $bc_1$ complex, substitution of 2–6 Pro residues in the hinge region greatly inhibited the activity (Table III, part A), which was considered

TABLE II

*Cell growth and electron transfer activity of the wild type and hinge region mutants of Synechococcus sp. PCC 7002*

Data reported with S.D. were obtained from three or more trials; data without S.D. were obtained from a single experiment. WT, wild type; ND, not done.

| Strain | Sequence | Growth (doubling time) | Half-time for cytochrome $f/c_6$ reduction | | |
|---|---|---|---|---|---|
| | | | No inhibitor | +DBMIB | |
| | | | | 2.5 μM | 20 μM |
| | | *h* | | *ms* | |
| WT | PPSSGGAGGG | 5.4 | 4 ± 0.4 | 260 ± 80[a] | 1070 |
| P44A/P45A | AASSGGAGGG | 5.6 | 3.7 ± 0.2 | 210 ± 30[a] | 1080 |
| S46G/S47G | PPGGGGAGGG | 5.3 | 3.1 ± 0.1 | 170 ± 40[a] | 730 |
| 4Pro | PPSSGPPPPG | 5.1 | 3.7 ± 0.2 | 320 ± 20 | 680 |
| 6Pro | PPPPGPPPPG | 6.2 | 9.6 ± 0.2 | 80 | ND |
| ΔA50 | PPSSGG_GGG | 4.8 | 4.4 ± 1.0 | 130 ± 10 | 410 |
| ΔS46–47 | PP__GGAGGG | 5.9 | 10 ± 2 | 12 ± 1 | 18 ± 2 |
| ΔG51–52 | PPSSGGA__G | 6.0 | 15 ± 1 | 17 ± 1 | 18 ± 1 |
| +2G-Δ2G | PPGGSSGGAG | 4.4 | 4.0 ± 0.2 | 200 ± 40 | 690 |
| +4Gly | PPSSGGAGGGGGGG | 5.2 | 4.8 ± 0.4 | 1800 ± 200 | 2240 |

[a] Reduction kinetics has two phases: a slow phase (≈70% in amplitude, $t_{1/2}$ shown) and a fast phase, ≈30% in amplitude, $t_{1/2}$ = 5 ms (for labeled data only).

key evidence in support of a functional requirement for mobility of the ISP soluble domain (19, 23, 41). Because flexibility of the ISP hinge region associated with the polyglycine sequence motif appears to be a conserved characteristic of the $b_6f$ complex hinge region (Table I), it was expected that a high degree of flexibility would be critical for the ISP movement. Surprisingly, decreasing the flexibility of the hinge region by substitution of 4 Pro residues for residues 49–52 (GAGG, mutant 4Pro) failed to inhibit the electron transfer rate of the complex ($t_{1/2}$ of cytochrome $f/c_6$ reduction = 3.7 ms) (Fig. 4 and Table II). A conformationally inflexible mutant was made by substitution of 2 additional proline residues for $Ser^{46}$ and $Ser^{47}$ in mutant 6Pro, resulting in a linker region with 8 Pro residues (including the native $Pro^{44}$ and $Pro^{45}$ residues) (Table II). There was a decrease in activity associated with this mutant, but the 2.4-fold decrease in the electron transfer rate ($t_{1/2}$ of cytochrome $f/c_6$ reduction = 9.6 ms) (Fig. 4 and Table II) was small considering the severity of the mutation and the effect of such mutations on the $bc_1$ complex (Table III, part A). Apparently, a high degree of rigidity in the hinge region is well tolerated in the $b_6f$ complex. The relatively small perturbation caused by a $Gly_6$-to-$Ala_6$ substitution, generated in other studies, has no effect on the function of the $b_6f$ complex in the green alga *Chlamydomonas reinhardtii* (42).

*Consequences of Shortening the Hinge Region*—In the bacterial and yeast cytochrome $bc_1$ complexes, deletion mutations in the ISP hinge region resulted in a 40–100% decrease in activity and often defects in assembly or stability (Table III, part C) (19, 23, 24, 26). In the $b_6f$ complex, the 1-residue deletion mutant ΔA50 displayed a phenotype similar to that of the wild type ($t_{1/2}$ of cytochrome $f/c_6$ reduction = 4.4 ms) (Fig. 4 and Table II), whereas the $bc_1$ complex was sensitive to a 1-residue deletion (Table III, part B). The rate of cytochrome $f/c_6$ reduction was decreased by factors of 2.5 and 4 compared with the wild type in the 2-residue deletion mutants ΔS46–47 ($t_{1/2}$ = 10 ms) and ΔG51–52 ($t_{1/2}$ = 15 ms) (Fig. 4 and Table II), respectively. Although the decreased activity of the hinge region mutant truncated by 2 residues implies that the minimum length for full activity is 7 residues, the 2-residue truncation mutation is not severe, as mutants could still grow and evolve oxygen at the wild-type rate (Fig. 5 and Table II). This is presumably because the rate-limiting step of electron transport under conditions of coupled phosphorylation for cell growth and $O_2$ evolution is slower than that under the uncoupled conditions of flash-induced turnover. Because deletion of 2 residues at two different positions in mutants ΔS46–47 and ΔG51–52 produced similar phenotypes, the observed effect of 2-residue deletions is attrib-

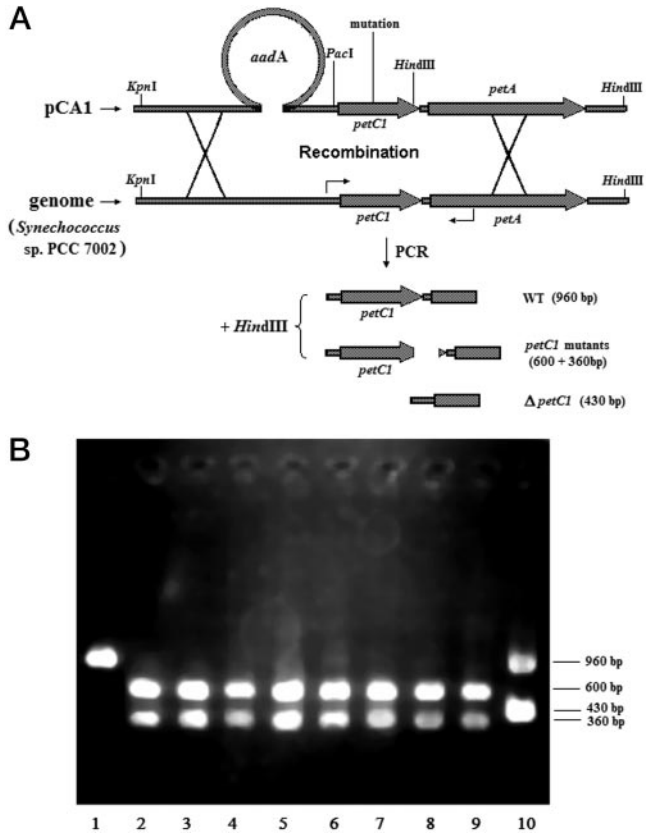


FIG. 3. *A*, strategy for the introduction of the *petC1* mutant into the *Synechococcus* sp. PCC 7002 genome and the detection of its segregation from the wild-type (*WT*) allele. After transformation, the plasmid pCA1, containing the entire *petCA* operon with a new *Hin*dIII site (silent mutation) at the 3′-end of *petC1*, an upstream *aadA* cassette, and a 1.5-kb 5′-flanking sequence, confers spectinomycin resistance on the host upon integration of the *aadA* cassette and its closely linked mutated *petC1* gene into the *Synechococcus* genome. The primary screening for complete segregants with the desired mutation in the *petC1* locus of the *Synechococcus* genome was performed by PCR and subsequent *Hin*dIII restriction analysis of the PCR product. *B*, PCR and *Hin*dIII restriction analysis of the genomic DNA from the wild type (*lane 1*) and mutants P44A/P45A (*lane 2*), S46G/S47G (*lane 3*), 4Pro (*lane 4*), ΔA50 (*lane 5*), ΔS46–47 (*lane 6*), ΔG51–52 (*lane 7*), +2G-Δ2G (*lane 8*), +4Gly (*lane 9*), and Δ*petC1* (*lane 10*). A 1-kb fragment containing *petC1* and the 5′-part of *petA* was amplified from the *Synechococcus* genomic DNA of the transformants by PCR with a forward primer (GGG CAA ACT AAG GCT C) and a reverse primer (AAA CTT GAT CGG GTA AAA CGG). The PCR product was digested with restriction enzyme *Hin*dIII and then analyzed by agarose gel electrophoresis.

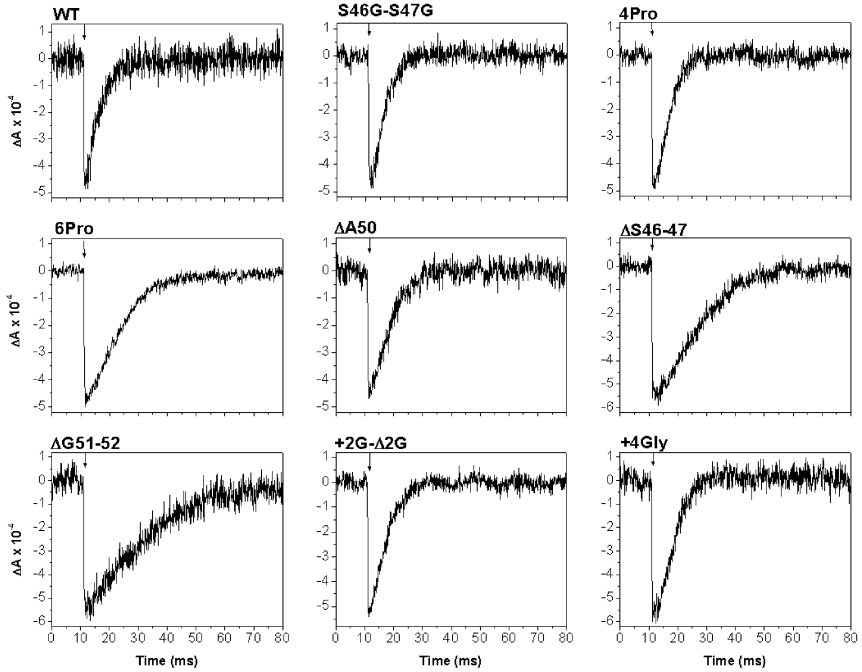


FIG. 4. **Kinetics of flash-induced cytochrome $f/c_6$ redox changes *in vivo* in the wild type and ISP hinge region mutants in the absence of inhibitors.** Each trace is an average of 36 flash-induced absorbance changes with 2 s of darkness between runs. $\Delta A$(cytochrome $f/c_6$) = $\Delta A$(556 nm) − $\Delta A$(540 nm). Cells were suspended at 5 μM chlorophyll in 5 mM HEPES (pH 7.5), 10 mM NaCl, and 10 mM $NaHCO_3$. 10 μM 3-(3,4-dichlorophenyl)-1,1-dimethylurea, 1 mM NHOH, 10 μM carbonyl cyanide *p*-trifluoromethoxyphenylhydrazone, and 1.0 mM KCN were added prior to measurements. Onset of flash is indicated by the *arrows*. The strain used for each measurement is shown at the top of each panel. *WT*, wild type.

TABLE III
*Comparison of effects of ISP hinge region mutations on cytochrome $bc_1$ and $b_6f$ complexes*

| Mutation | Effects on activity and $Q_p$ site integrity | |
|---|---|---|
| | $bc_1$ (from literature) | $b_6f$ (this work) |
| A. Substitution | | |
| 2–6 Pro (decreased flexibility) | Greatly decreased activity (19, 23). | No effect for 4 Pro; slightly decreased activity for 6 Pro |
| 2–6 Gly (increased flexibility) | Greatly decreased activity for 6 Gly (19) | No effect for 2 Gly (already 5 Gly in wild type) |
| B. Elongation | | |
| 1 residue | Decreased activity (17, 26); slightly resistant to stigmatellin in yeast (26). | No effect |
| 2–4 residues | Greatly decreased activity (17, 26) | No effect on activity; increased sensitivity to DBMIB and stigmatellin for 4-Gly insertion |
| C. Truncation | | |
| 1 residue | Decreased activity (19, 26); slightly resistant to stigmatellin (26) | No effect |
| 2–3 residues | Decreased activity (19, 23, 24, 26); alteration in EPR signal (23) | Decreased activity; highly resistant to DBMIB and stigmatellin |

uted to truncation in length instead of a positional effect. This was confirmed by the restoration mutant +2G-Δ2G for mutant ΔG51–52, in which the reinsertion of 2 Gly residues at a second site between $Pro^{45}$ and $Ser^{46}$ could fully revert the loss of function in ΔG51–52 (Fig. 4 and Table II). The inference that 7 residues is the minimum length of the hinge region that retains full function is confirmed by studies with $Q_p$ site inhibitors.

*Sensitivity of Hinge Region Mutants to $Q_p$ Site Inhibitors*—Electron transfer activity was measured after flash excitation in the presence of the $Q_p$ site inhibitors DBMIB and stigmatellin. The wild type and mutants P44A/P45A, S46G/S47G, 4Pro, ΔA50, and +2G-Δ2G were sensitive to DBMIB to a similar extent (Table II). 2.5 and 20 μM DBMIB inhibited cytochrome $f/c_6$ re-reduction, slowing the reduction half-times for these strains from 3–5 ms to 130–260 and 410–1080 ms, respectively. Mutant 6Pro was slightly less sensitive to DBMIB, with 2.5 μM DBMIB slowing the reduction half-time from 9.6 to 80 ms (Table II). However, the 2-residue truncation mutants ΔS46−47 and ΔG51–52 were insensitive to DBMIB (Table II). 20 μM DBMIB inhibited cytochrome $f/c_6$ re-reduction only slightly, slowing the half-times in mutants ΔS46−47 and ΔG51–52 from 10 to 18 ms and from 15 to 18 ms, respectively. The loss of inhibitor sensitivity in the latter mutant was reverted in the restoration mutant +2G-Δ2G (Table II). A similar result was obtained for $O_2$ evolution, where 2.5 μM DBMIB caused >95% inhibition in the wild type, but only ~30% in mutants ΔS46−47 and ΔG51–52 (Fig. 5). Similarly, the cytochrome $b_6f$ complexes in mutants ΔS46−47 and ΔG51–52 were insensitive to stigmatellin. 10 μM stigmatellin caused an ~10-fold decrease in the cytochrome $f/c_6$ reduction rate in the wild type, but only an ~1.5-fold decrease in these two mutants (Fig. 6). The loss of sensitivity to $Q_p$ site inhibitors in the 2-residue truncation mutant is consistent with structure data showing that the cluster-binding subdomain of the ISP is required to form the inhibitor-binding site, the $Q_p$ site (Fig. 1). It is inferred that a hinge region shorter than 7 residues results in insufficient contact between the ISP cluster-binding region, the membrane surface, and an altered $Q_p$ site.

In contrast to the loss of inhibitor sensitivity in the 2-residue deletion mutants, the $b_6f$ complex became more sensitive to $Q_p$ site inhibitors in mutant +4Gly. 2.5 μM DBMIB caused an ~70-fold decrease in the cytochrome $f/c_6$ reduction rate in the wild type and an almost 400-fold decrease in mutant +4Gly (Table II). A similar result was also obtained in flash experiments with stigmatellin (Fig. 6). Thus, the pronounced elongation allows a different fit of the ISP to the $Q_p$-binding niche, resulting in an increase in affinity for quinol analog inhibitors, but changes in distance from the $Q_p$ site quinol to the [2Fe-2S] cluster and its ligands are small enough that the measured electron transfer rate is not affected.

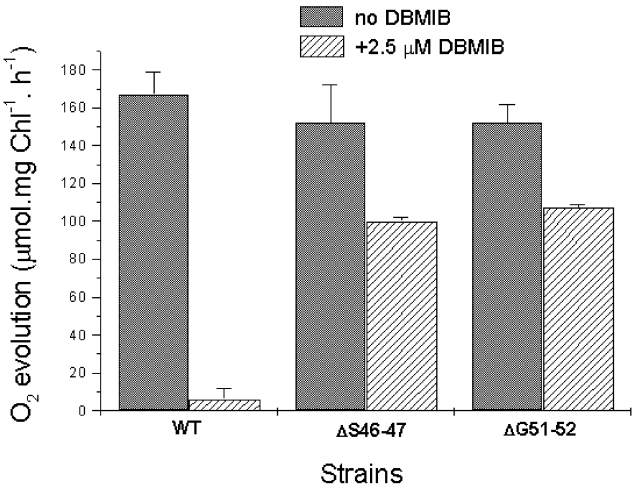


FIG. 5. **Oxygen evolution rates of the wild-type and mutant ΔS46–47 and ΔG51–52 cells in the absence and presence of 2.5 μM DBMIB.** Oxygen evolution rates were measured at 39 °C as described under "Materials and Methods." *Chl*, chlorophyll; *WT*, wild type.

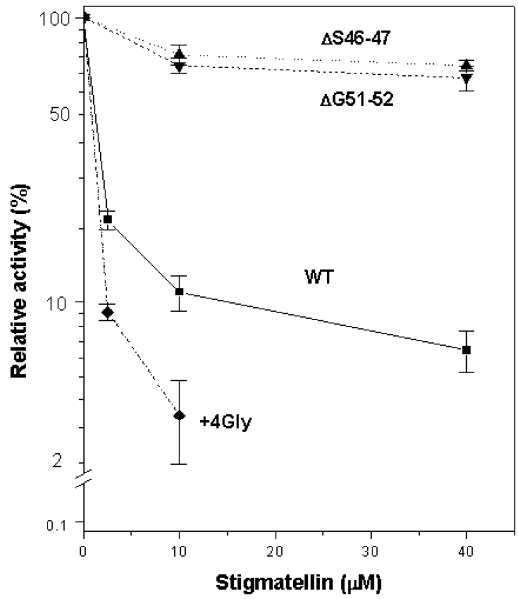


FIG. 6. **Effect of stigmatellin on the electron transfer activity of the $b_6f$ complex in the wild-type and mutants ΔS46–47, ΔG51–52, and +4Gly.** The relative electron transfer activity of the $b_6f$ complex as a function of stigmatellin concentration is expressed as a ratio of the flash-induced re-reduction rates of cytochrome $f/c_6$ measured in the presence and absence of stigmatellin. Flash kinetic measurements were performed as described in the legend to Fig. 4. *WT*, wild type.

## DISCUSSION

*Insensitivity of the $b_6f$ Complex to Hinge Region Structure Changes: Implications for Function*—The $bc_1$ and $b_6f$ complexes display a very different sensitivity to changes in flexibility and increases in length of their hinge regions (Table III, parts A and B). Decreasing the flexibility of the hinge region by substitution of 2–6 Pro residues or introduction of a disulfide bond in this region caused a large decrease in the activity of the $bc_1$ complex, consistent with the concept that these changes hamper the mobility and movement of the ISP soluble domain (19, 22, 23). However, the deleterious effects of an increase in flexibility of the hinge region by substitution of 6 Gly residues (19) and of increases in length by insertion of 1–3 Ala residues (17, 24, 26) are not readily explained by the x-ray structures or the concept of preservation of ISP mobility. Indeed, although x-ray structure data led to the concept of the mobile ISP as an essential component in the high potential electron transport pathway for quinol oxidation (7, 12–16), these structure data do not at present elucidate the mechanism that drives and controls the ISP motion. The hinge region mutagenesis data in the $bc_1$ complex imply that there is an optimum structure of the hinge region for mobility and function. In the $b_6f$ complex, the 8-residue ISP hinge region consists mostly of Gly residues and is presumably more flexible than that in the $bc_1$ complex (Table I). The present study indicates that an optimum flexibility and length of the hinge region are not required for the function of the $b_6f$ complex. It can be mutated to be conformationally more flexible, extremely rigid (up to substitution of 6 Pro residues), or 4 residues longer without significant effect on function (Tables II and III). The large difference between the $b_6f$ and $bc_1$ complexes in their responses to structure changes in the ISP hinge region implies a significant difference in the mechanism and/or amplitude of the ISP movement in the two complexes.

*Physical Properties of ISP Motion*—In the crystal structures of the $bc_1$ complex, the hinge region is uncoiled and extended when the ISP [2Fe-2S] cluster is in the quinol-proximal position ($Q_p$ or "*b*" position), whereas it curls up in a helical conformation when it is proximal to cytochrome $c_1$ (Fig. 1) (12, 14, 15). It is not clear whether such a secondary structure change in the hinge region is a driving force for, or solely a result of, the ISP domain movement in the $bc_1$ complex. Considering the large differences between the $bc_1$ and $b_6f$ complexes in the structures of their hinge regions and their responses to hinge region mutations, it is very likely that formation of the helix in the $bc_1$ ISP hinge region is needed to drive the reduced ISP [2Fe-2S] cluster away from the $Q_p$ site toward the "$c_1$" position, whereas such a driving device is apparently absent in the $b_6f$ complex. This hypothesis would explain the observation in the $bc_1$ structures that the ISP is in an intermediate or $c_1$ position in the absence of stigmatellin (12, 14) because of favorable helix formation in the hinge region. It also explains the high sensitivity of the $bc_1$ complex to changes in flexibility and increases in length of the hinge region. Changes in flexibility by Pro or Gly substitutions or introduction of a disulfide bond in the hinge region (19, 22, 23) would interrupt the formation of $\alpha$-helical structure in the hinge region and thus impair ISP movement. An increase in hinge length (17, 24, 26) would decrease the tension in the hinge region, making it unable to tug the ISP away from $Q_p$ site, as was suggested previously (16). In the case of the hinge region of the $b_6f$ complex in wild-type *Synechococcus* sp. PCC 7002, it should be essentially structure-less because of the presence of 5 Gly residues and 2 adjacent Pro residues (Table I), implying that secondary structure change or tension in the linker region is not required for ISP domain movement in the $b_6f$ complex. Therefore, excess flexibility and length are not inhibitory. However, the finding that the large decreases in hinge flexibility by substitution of 4–6 Pro residues have at most a small effect on the function of the $b_6f$ complex is surprising. It suggests that hinge flexibility is less important than in the $bc_1$ complex.

Why is a coil-helix transition mechanism not required, and a high degree of hinge rigidity allowed in the $b_6f$ complex? We propose two alternative explanations. (i) A structural barrier for ISP movement that is present in the $bc_1$ complex is absent or smaller in the $b_6f$ complex. The "*ef* loop" in the $bc_1$ complex connects the most separated transmembrane helices, E and F, of cytochrome *b* on the *p* side of the membrane and holds the ISP soluble domain and cytochrome $c_1$ in the correct orientation for ISP movement and electron transfer. Substitution of Phe for $Leu^{286}$ (located around site *b* in Fig. 2*A*) in the *ef* loop can partially overcome the defect in ISP movement in mutant +1Ala of *R. capsulatus*, indicating that this surface loop rep-

resents the major physical barrier to ISP domain movement from the $Q_p$ site to the $c_1$ position (21). Leu$^{286}$ (Leu$^{262}$ in the bovine complex) is highly conserved in the $bc_1$ complex, but is substituted with a highly conserved Phe (Phe$^{69}$ in subunit IV in *Synechococcus* PCC 7002) in the $b_6f$ complex. Thus, the physical barrier in the *ef* loop of the $bc_1$ complex may be absent in the $b_6f$ complex. In the absence of the barrier, the coil-helix transition of the hinge region may not be required to pull the ISP from the $Q_p$ site to the $c_1$ positions.

(ii) The studies on changes in orientation of the [2Fe-2S] cluster in the presence and absence of DBMIB (27) show that the ISP movement is sufficient to reorient the principle g value transitions of the [2Fe-2S] cluster. However, the amplitude of the ISP cluster motion may be significantly smaller than the 60 °-16 Å rotation-translation inferred for the $bc_1$ complex. A smaller amplitude would allow decreased flexibility and smaller conformational constraints in the hinge region. An important structure difference between the $b_6f$ and $bc_1$ complexes is that the electron acceptors of the ISP, cytochromes *f* and $c_1$, respectively, are completely different in sequence and structure (10, 11) and heme orientation (43–46). A close orientation of the cytochrome *f* heme to the ISP [2Fe-2S] cluster would eliminate the necessity of large-scale ISP movement; on the other hand, a steric constraint from cytochrome *f* on the free space for ISP movement would prevent large-scale ISP movement, although a significant displacement of the ISP [2Fe-2S] cluster from the quinol of the $Q_p$ site is still required for a bifurcated electron transport chain in both cases (7).

*Minimum Length of the Hinge Region Required for Optimum Binding of ISP at the $Q_p$ Site*—The loss of sensitivity of the $b_6f$ complex to the $Q_p$ site inhibitors in the 2-residue truncation mutants is striking. Previously, only a small (50%) increase in the $I_{50}$ of stigmatellin was reported for a 1-residue truncation mutant of the yeast mitochondrial $bc_1$ complex (26), and no information on changes in inhibitor sensitivity was provided from studies on photosynthetic bacteria (Table III) (17–19, 21–23). However, alterations in EPR spectra of the ISP were observed in some $bc_1$ hinge region truncation mutants of the bacteria (19, 23). These results indicate that truncation of the hinge region has a direct impact on the structure of the $Q_p$ site in both the $b_6f$ and $bc_1$ complexes. The observed decrease in $b_6f/bc_1$ activity in these truncation mutants can be readily explained by defects in the $Q_p$ site that also result in a decrease in the $K_m$ of quinol, as was observed in the yeast mitochondrial $bc_1$ complex (26).

Examination of the interaction between the ISP soluble domain and the *p* side of cytochrome *b* in the presence of stigmatellin indicates that a minimum hinge length is sterically required for the proper docking of the [2Fe-2S] cluster region at the $Q_p$ site. In the structure, the ISP soluble domain resembles a lever, with the [2Fe-2S] cluster region located at one end and the hinge region linked to the other end (Fig. 2*A*). In the middle, the ISP $\beta_{2-3}$-strand region (site *a* in Fig. 2) is positioned close to the *ef* loop of cytochrome *b* (site *b* in Fig. 2) to form a "fulcrum region" (Fig. 2). Because of the steric repulsion between the ISP and cytochrome *b* in the fulcrum region, the moving and binding of the [2Fe-2S] cluster region to the membrane ($Q_p$ site) would lead to displacement of the other end of the ISP soluble domain and elongation of the hinge region. Vice versa, truncation of the hinge region would hinder the movement and binding of the [2Fe-2S] cluster region to the $Q_p$ site. This fulcrum region in the $bc_1$ complex may also work as the "structure barrier region" of the ISP domain movement proposed in Ref. 21 (see discussion above). The structure and orientation of the $\beta_{2-3}$-strand region are similar in the $bc_1$, $b_6f$, and archaeal Rieske ISPs (9, 47). A similar pattern of interaction between the ISP soluble domain and the *p* side of cytochrome $b_6$/subunit IV was observed in the modeled structure of the $b_6f$ complex (Fig. 2*B*). Thus, it is inferred that a minimum length of 7 residues in the ISP hinge region is required for optimum binding of the ISP at the $Q_p$ site in the $b_6f$ complex. The decrease in activity and the loss of $Q_p$ site inhibitor sensitivity in the 2-residue truncation mutants may be explained by the requirement for H-bonding of quinol and stigmatellin to the His$^{129}$ (equivalent to His$^{161}$ in bovine) ligand of the [2Fe-2S] cluster for efficient electron transfer from quinol to ISP and inhibitor binding (12, 15, 48). A truncation of the hinge region would not allow close approach of the [2Fe-2S] cluster at the $Q_p$ site and would thus impair the formation of this H-bond.

*Acknowledgments*—We are grateful to G. M. Soriano and H. Zhang for helpful advice and discussions and T. Kallas and W. R. Widger for kind gifts of the *Synechococcus* sp. PCC 7002 wild-type strain and plasmid pUHWRW1, respectively.

REFERENCES

1. Kallas, T. (1994) in *The Molecular Biology of Cyanobacteria* (Bryant, D. A., ed) pp. 259–317, Kluwer Academic Publishers Group, Dordrecht, The Netherlands
2. Soriano, G. M., Ponamarev, M. V., Carrell, C. J., Xia, D., Smith, J. L., and Cramer, W. A. (1999) *J. Bioenerg. Biomembr.* **31,** 201–213
3. Zhang, H., Whitelegge, J. P., and Cramer, W. A. (2001) *J. Biol. Chem.* **276,** 38159–38165
4. Whitelegge, J. P., Zhang, H., Aguilera, R., Taylor, R. M., and Cramer, W. A. (2002) *Mol. Cell. Proteomics* **1,** 816–827
5. Widger, W. R., Cramer, W. A., Herrmann, R. G., and Trebst, A. (1984) *Proc. Natl. Acad. Sci. U. S. A.* **81,** 674–678
6. Link, T. A. (1997) *FEBS Lett.* **412,** 257–264
7. Crofts, A. R., Guergova-Kuras, M., Huang, L., Kuras, R., Zhang, Z., and Berry, E. A. (1999) *Biochemistry* **38,** 15791–15806
8. Soriano, G. M., and Cramer, W. A. (2001) *Biochemistry* **40,** 15109–15116
9. Carrell, C. J., Zhang, H., Cramer, W. A., and Smith, J. L. (1997) *Structure* **5,** 1613–1625
10. Martinez, S. E., Huang, D., Ponomarev, M., Cramer, W. A., and Smith, J. L. (1996) *Protein Sci.* **5,** 1081–1092
11. Soriano, G. M., Smith, J. L., and Cramer, W. A. (2001) in *Handbook of Metalloproteins* (Messerschmidt, A., Huber, R., Wieghardt, K., and Poulos, T., eds) pp. 172–181, John Wiley & Sons Ltd., London
12. Zhang, Z., Huang, L., Shulmeister, V. M., Chi, Y. I., Kim, K. K., Hung, L. W., Crofts, A. R., Berry, E. A., and Kim, S. H. (1998) *Nature* **392,** 677–684
13. Kim, H., Xia, D., Yu, C. A., Xia, J. Z., Kachurin, A. M., Zhang, L., Yu, L., and Deisenhofer, J. (1998) *Proc. Natl. Acad. Sci. U. S. A.* **95,** 8026–8033
14. Iwata, S., Lee, J. W., Okada, K., Lee, J. K., Iwata, M., Rasmussen, B., Link, T. A., Ramaswamy, S., and Jap, B. K. (1998) *Science* **281,** 64–71
15. Hunte, C., Koepke, J., Lange, C., Rossmanith, T., and Michel, H. (2000) *Structure* **8,** 669–684
16. Berry, E. A., Guergova-Kuras, M., Huang, L. S., and Crofts, A. R. (2000) *Annu. Rev. Biochem.* **69,** 1005–1075
17. Darrouzet, E., Valkova-Valchanova, M., Moser, C. C., Dutton, P. L., and Daldal, F. (2000) *Proc. Natl. Acad. Sci. U. S. A.* **97,** 4567–4572
18. Darrouzet, E., Valkova-Valchanova, M., and Daldal, F. (2002) *J. Biol. Chem.* **277,** 3464–3470
19. Darrouzet, E., Valkova-Valchanova, M., and Daldal, F. (2000) *Biochemistry* **39,** 15475–15483
20. Darrouzet, E., Moser, C. C., Dutton, P. L., and Daldal, F. (2001) *Trends Biochem. Sci.* **26,** 445–451
21. Darrouzet, E., and Daldal, F. (2002) *J. Biol. Chem.* **277,** 3471–3476
22. Tian, H., White, S., Yu, L., and Yu, C. A. (1999) *J. Biol. Chem.* **274,** 7146–7152
23. Tian, H., Yu, L., Mather, M. W., and Yu, C. A. (1998) *J. Biol. Chem.* **273,** 27953–27959
24. Obungu, V. H., Wang, Y., Amyot, S. M., Gocke, C. B., and Beattie, D. S. (2000) *Biochim. Biophys. Acta* **1457,** 36–44
25. Ghosh, M., Wang, Y., Ebert, C. E., Vadlamuri, S., and Beattie, D. S. (2001) *Biochemistry* **40,** 327–335
26. Nett, J. H., Hunte, C., and Trumpower, B. L. (2000) *Eur. J. Biochem.* **267,** 5777–5782
27. Schoepp, B., Brugna, M., Riedel, A., Nitschke, W., and Kramer, D. M. (1999) *FEBS Lett.* **450,** 245–250
28. Roberts, A. G., Bowman, M. K., and Kramer, D. M. (2002) *Biochemistry* **41,** 4070–4079
29. Heimann, S., Ponamarev, M. V., and Cramer, W. A. (2000) *Biochemistry* **39,** 2692–2699
30. Lee, T., Metzger, S. U., Cho, Y. S., Whitmarsh, J., and Kallas, T. (2001) *Biochim. Biophys. Acta* **1504,** 235–247
31. Buzby, J. S., Porter, R. D., and Stevens, S. E., Jr. (1985) *Science* **230,** 805–807
32. Ponamarev, M. V., Schlarb, B. G., Howe, C. J., Carrell, C. J., Smith, J. L., Bendall, D. S., and Cramer, W. A. (2000) *Biochemistry* **39,** 5971–5976
33. Widger, W. R. (1991) *Photosynth. Res.* **30,** 71–84
34. Goldschmidt-Clermont, M. (1991) *Nucleic Acids Res.* **19,** 4083–4089
35. Berthold, D. A., Best, B. A., and Malkin, R. (1993) *Plant Mol. Biol. Reports* **11,** 338–344
36. Ponamarev, M. V., and Cramer, W. A. (1998) *Biochemistry* **37,** 17199–17208
37. Cramer, W. A., Martinez, S. E., Huang, D., Tae, G. S., Everly, R. M., Heymann,

J. B., Cheng, R. H., Baker, T. S., and Smith, J. L. (1994) *J. Bioenerg. Biomembr.* **26,** 31–47
38. Guex, N., and Peitsch, M. C. (1997) *Electrophoresis* **18,** 2714–2723
39. Schneider, D., Skrzypczak, S., Anemuller, S., Schmidt, C. L., Seidler, A., and Roegner, M. (2002) *J. Biol. Chem.* **277,** 10949–10954
40. Baymann, F., Rappaport, F., Joliot, P., and Kallas, T. (2001) *Biochemistry* **40,** 10570–10577
41. Sadoski, R. C., Engstrom, G., Tian, H., Zhang, L., Yu, C. A., Yu, L., Durham, B., and Millett, F. (2000) *Biochemistry* **39,** 4231–4236
42. de Vitry, C., Finazzi, G., Baymann, F., and Kallas, T. (1999) *Plant Cell* **11,** 2031–2044
43. Bergstrom, J., and Vanngard, T. (1982) *Biochim. Biophys. Acta* **682,** 452–456
44. Crowder, M. S., Prince, R. C., and Bearden, A. (1982) *FEBS Lett.* **144,** 204–208
45. Mosser, G., Breyton, C., Olofsson, A., Popot, J.-L., and Rigaud, J. L. (1997) *J. Biol. Chem.* **272,** 20263–20268
46. Schoepp, B., Chabaud, E., Breyton, C., Vermeglio, A., and Popot, J.-L. (2000) *J. Biol. Chem.* **275,** 5275–5283
47. Bonisch, H., Schmidt, C. L., Schafer, G., and Ladenstein, R. (2002) *J. Mol. Biol.* **319,** 791–805
48. Samoilova, R. I., Kolling, D., Uzawa, T., Iwasaki, T., Crofts, A. R., and Dikanov, S. A. (2002) *J. Biol. Chem.* **277,** 4605–4608
49. Kraulis, P. J. (1991) *J. Appl. Crystallogr.* **24,** 946–950
50. Merritt, E. A., and Murphy, M. E. P. (1994) *Acta Crystallogr. Sect. D Biol. Crystallogr.* **50,** 869–873
51. Iwata, S., Saynovits, M., Link, T. A., and Michel, H. (1996) *Structure* **4,** 567–579
52. Zhang, H., Carrell, C. J., Huang, D., Sled, V., Ohnishi, T., Smith, J. L., and Cramer, W. A. (1996) *J. Biol. Chem.* **271,** 31360–31366